

Nonlocality-driven switchable fast-slow light effect in hyperbolic metamaterials in epsilon-near-zero regime

V. B. Novikov^{1,*}, A. P. Leontiev^{2,3}, K. S. Napolskii^{2,3} and T. V. Murzina¹

¹*Department of Physics, M.V. Lomonosov Moscow State University, Moscow 119991, Russia*

²*Department of Materials Science, M.V. Lomonosov Moscow State University, Moscow 119991, Russia*

³*Department of Chemistry, M.V. Lomonosov Moscow State University, Moscow 119991, Russia*



(Received 10 August 2022; revised 30 September 2022; accepted 3 October 2022; published 13 October 2022)

The recent surge of optics of hyperbolic metamaterials (HMMs) has been fueled by their fascinating optical properties, one of the most intriguing being their strong optical nonlocality. In this work we demonstrate that in metal nanorod-based HMMs the nonlocality results in fast and slow light effects in the propagation of femtosecond laser pulses in close spectral vicinity of the HMM epsilon-near-zero regime. These effects are switchable via the angle of incidence and light wavelength. We elucidate that revealed dynamical phenomena stem from the zero-transmission points of HMM and related phase singularities caused by the destructive interference of the main optical wave and the additional wave mediated by the spatial dispersion of light in the HMMs.

DOI: [10.1103/PhysRevB.106.165415](https://doi.org/10.1103/PhysRevB.106.165415)

I. INTRODUCTION

Optics of hyperbolic metamaterials (HMMs) is on the cutting edge of modern photonics due to their unusual optical properties. Being a uniaxial birefringent media, HMMs are characterized by strong optical anisotropy with opposite signs of principal dielectric tensor components. This results in exotic hyperbolic dispersion of light in HMMs related to the high density of photonic states and support of high- k waves [1]. Another exciting feature of HMMs is the epsilon-near-zero (ENZ) regime when permittivity in a particular direction becomes close to zero, which can be harnessed for a great boost of electric field strength within the HMMs. These properties make HMMs a promising platform for nonlinear optics [2], superresolution imaging [3,4] and related photolithography [5], broadband absorption [6], control of radiation pattern [7], and enhancement of magneto-optical effects [8], to name a few.

A wealth of optical effects in HMMs are realized typically in their material design consisting in subwavelength-thick metal/dielectric multilayers or an array of metal nanorods in a dielectric matrix [9]. As the HMMs are constructed at the subwavelength scale, the effective medium description of their dielectric properties can be applied [10–14]. In turn, nanostructuring of optical media can bring about optical nonlocality and related spatial dispersion, i.e., the dependence of the effective permittivity tensor on the wave vector $\hat{\epsilon}(\omega, \mathbf{k})$ [15],

$$\epsilon_{ij}(\omega, \mathbf{k}) = \epsilon_{ij}(\omega) + i\gamma_{ijk}(\omega)k_k + \alpha_{ijkl}(\omega)k_k k_l + \dots, \quad (1)$$

providing additional nonlocality-based control of light, e.g., by inducing chirality in highly symmetric lattices [16]. In contrast to most natural materials, in which nonlocality is

a gentle effect [17], in artificial hyperbolic media such as nanorod-based and multilayered HMMs it becomes quite strong [10,18]. It has sparked extensive research efforts for taming the nonlocality of multilayered HMMs for the advanced manipulation of light, resulting in a spectral shift of the enhancement of the Goos-Hänchen effect [19], nonlocality-mediated surface waves [20], beam splitting [18,21], and anomalous transmission in the vicinity of the total internal reflection angle [22]. Spatial dispersion is a limiting factor for the cutoff of hyperbolicity of the light dispersion in HMMs [10,23] and becomes significant for light focusing by HMM hyperlenses [24]. Recently nonlocality in multilayered HMMs has been used for the control of light emission, providing a nonzero Cherenkov threshold [25] in contrast to thresholdless Cherenkov radiation in local HMMs [26] and tuning (i) the spectral shift of emission of a dye layer covering the HMM and (ii) the charge transfer dynamics in organic semiconductors [27,28]. Nonlocality is intrinsic to optical hyperbolic metamaterials and appears as well in other HMM designs, e.g., in hyperbolic graphene-based metasurfaces [29] and fishnet structures [30]. In the gigahertz frequency range the nonlocality of response is achieved by using advanced methods based on the corrugated wires supporting spoof plasmons [31].

Plenty of the abovementioned phenomena are mediated by the appearance of the so-called additional wave driven by HMM spatial dispersion [32]. It appears along with the main modes associated with ordinary and extraordinary waves in anisotropic HMM media. According to Eq. (1), in the ENZ regime when the permittivity goes to zero, the effect of spatial dispersion is especially strong, so this additional wave has a dramatic effect on the light transmission [11,33]. It appears as well in natural materials near the exciton absorption line, which brings about strong optical nonlocality [34]. Curiously, nonlocality in isotropic ENZ materials can be used for two-plasmon spontaneous emission [35].

*vb.novikov@physics.msu.ru

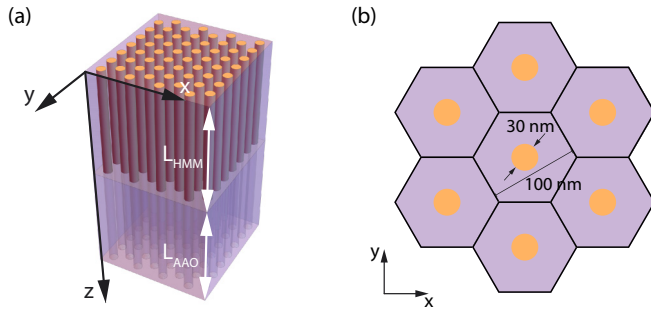


FIG. 1. (a) Scheme of the experimental structure and (b) cross section of the HMM. Hexagons illustrate primitive unit cells of the nanorod array.

The ENZ regime of HMMs facilitates the enhancement of the nonlinear optical interaction [36,37] that enables superior possibilities for nonlinear steering of laser pulses, as was predicted for multilayered structures [38] and demonstrated experimentally in metal nanorod-based HMMs [39]. In this aspect the pulse dynamics in HMMs could be of paramount importance. Recent years have witnessed efforts toward exploiting hyperbolic dispersion in HMMs for laser pulse control. The slow-down of light was predicted for the multilayered HMM waveguides [40,41], while it was proposed theoretically that the coupling between forward and backward eigenmodes in nanorod-based HMM waveguides can be used for fast and slow pulse propagation [42]. At the same time, to date there have been quite a few experimental works on the specific role of hyperbolic dispersion in optical pulse propagation through HMMs [43–45]. Thus, slow light appears in thin hexagonal boron nitride layers supporting hyperbolic dispersion of phonon polaritons [43]. Very recently pioneering observation of the pulse advance and delay effects in metal nanorod-based HMMs due to the topological transition from elliptic to hyperbolic dispersion was reported [44]. To the best of our knowledge, in spite of promising applications of HMMs for laser pulse control, the effects of optical nonlocality and related spatial dispersion in HMMs have not been considered in detail in the pulse propagation except for a very recent paper [45], which, however, left the mechanism of the specific pulse dynamics in nonlocal HMM under veil.

In this work we experimentally and theoretically investigate the effect of ENZ-assisted optical nonlocality of metal nanorod-based HMMs on the dynamics of propagating femtosecond laser pulses. We demonstrate that the destructive interference of the main and additional modes within the HMM is decisive in the pulse dynamics resulting in the fast and slow light effects mediated by phase singularities of the HMM transmittance. The effect of the pulse chirp in light dynamics is considered.

II. EXPERIMENTAL DETAILS

A. Experimental nanostructures

Experiments were carried out for the HMMs consisting of arrays of silver nanorods grown in the anodic aluminium oxide (AAO) template [Fig. 1(a)]. Details of the fabrication

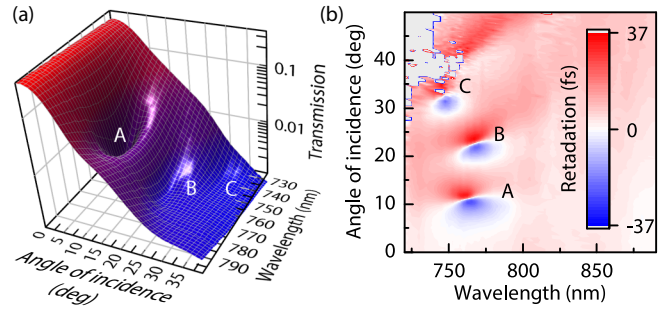


FIG. 2. Measured $\lambda - \theta$ dependencies of (a) p -polarized light transmittance of the HMM and (b) pulse delay in the HMM. Letters indicate the transmittance dips and related delay features. The gray region is out of the sensitivity of the experimental setup.

procedure can be found in Ref. [46]. Nanorods with a diameter of $d = 30$ nm were ordered at the short range in a hexagonal lattice with the spacing of $a = 100$ nm, which corresponds to the metal fraction in the nanocomposite of $f = 8\%$ [Fig. 1(b)]. The hexagonal package of nanorods was set by pore ordering in the AAO template formed in the electrochemical etching process [47]. The thickness of the HMM film was about $L_{\text{HMM}} = 1050 \pm 240$ nm. The unfilled part of AAO template with the thickness of $L_{\text{AAO}} = 50$ μm served as the mechanical support substrate [Fig. 1(a)]. Thermal annealing, proven to reduce optical losses in electrodeposited metal [48], was not applied here because of the good plasmonic properties of silver and its chemical reactivity.

This metamaterial exhibits the ENZ regime in the spectral vicinity of the wavelength of $\lambda_{\text{ENZ}} = 760$ nm (Sec. I in Supplemental Material [49]) that appears as a pronounced decrease of the transmission (T) of the p -polarized light with increasing angle of incidence (θ), as shown in Fig. 2(a). It is worth noting the set of transmission dips [marked by letters in Fig. 2(a)], which we argue are the result of optical nonlocality of the considered HMM. We note that the observed astonishing minima are well pronounced owing to (i) the measurement of the HMM transmission using parallel incident light beam without focusing and (ii) the large length of the metal nanorods. The former eliminates the smearing of the dips caused by the spatial spectrum of incident light, and the latter provides multiple transmission minima in moderate range of the angle of incidence.

B. Fast-slow light effect in HMM

For the HMM described above we investigated the dynamics of the transmission of 80 fs laser pulses generated by a titanium-sapphire laser (Avesta) with the central wavelength λ tunable in the range of 740–890 nm. A parallel unfocused laser beam with the size of 3×1 mm² molded by the slit aperture was incident on the HMM, and the pulse delay in the metamaterial was measured using the nonlinear cross-correlation method; the details of this procedure can be found elsewhere. In brief, the laser pulse was divided by a beam splitter into signal and reference arms. The signal pulse passed through the HMM, and the reference one was retarded by the delay line, so the second harmonic power appeared under the cross interaction of the signal and ref-

erence pulses in the beta barium borate (BBO) crystal and gave the intensity cross-correlation function. To extract the pulse delay attributed solely to the HMM layer, we measured the spectral-angular map of the pulse retardation in porous AAO substrate. Then the pulse delay (τ) in the HMM was obtained as the difference of both retardations of maxima of the cross-correlation functions. Figure 2(b) shows the resultant wavelength-angle map of τ induced by the HMM.

We revealed the conspicuous change of τ in the spectral vicinity of the ENZ regime of the HMM, which exhibits both fast and slow light effects corresponding to the negative and positive values of τ , respectively. The HMM reveals the pulse advance up to 28 fs and the retardation of 36 fs that correspond to the group refractive index of $n_g = -6$ and 11, respectively. As seen, these dynamical effects change one another with varying θ . The enthralling point here is the matching of the $\lambda - \theta$ position of the fast-slow light and the HMM transmission dips. It should be noted that the found astounding superluminality does not contradict the special theory of relativity, as this effect is revealed for the advance of the pulse maximum rather than the pulse leading front [50]. We note that previously the fast-slow light effects were found in various isotropic local media, e.g., in solids, gases, and atomic vapors supporting resonant dispersion related to the atomic transitions [51,52] or caused by the application of sophisticated approaches based on the electromagnetically induced absorption/transmission [53,54], coherent population oscillations [55], stimulated Brillouin scattering [56], and gain-assisted superluminality [57].

III. THEORY

A. Laser pulse transmission in HMM

Fast-slow light effects observed in the experiment are confirmed by numerical simulations of the pulse transmission through the HMM film when taking into account the spatial dispersion of light in the metamaterials. We consider the incidence under the angle of θ of both unchirped and chirped p -polarized laser pulses with the temporal dependence of the electric field amplitude given by

$$E_{\text{inc}}(t) = \frac{1}{\sqrt{V}} \exp(-[1/(2V^2)](t/\sigma)^2 + i\varphi) \exp(-i\omega t), \quad (2)$$

where $V = \sqrt{1 + \beta^2}$, chirp modulation phase is $\varphi = [\beta/(2V^2)](t/\sigma)^2$, and β is the dimensionless chirp parameter [58]. Positive β corresponds to the higher frequency at the leading pulse edge. In simulations we assumed $\sigma = 80 \text{ fs}/(2\sqrt{\ln(2)})$ that corresponds to 80 fs full width at half maximum (FWHM) intensity of unchirped pulse. We obtained the temporal dependence of the electric field of the transmitted laser pulse using the inverse Fourier transform

$$E(t) = \mathcal{F}^{-1}[E_{\text{inc}}(\omega)t(\omega, \theta)], \quad (3)$$

where $E_{\text{inc}}(\omega)$ is the Fourier amplitude of $E_{\text{inc}}(t)$ and $t(\omega, \theta)$ is the field transmission coefficient of HMM film for the p -polarized plane wave of the frequency ω incident at the angle θ . Details of the calculations of $t(\omega, \theta)$ are given below in Sec. III B.

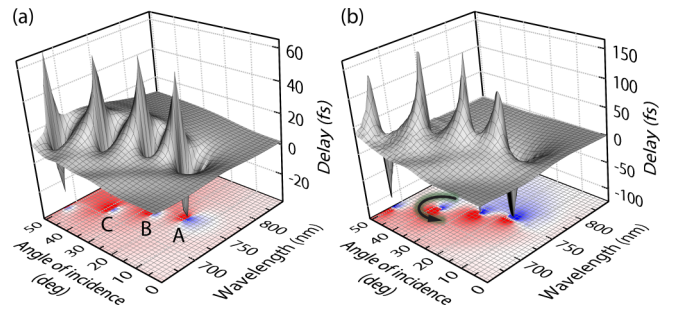


FIG. 3. Calculated $\lambda - \theta$ dependence of the delay of the laser pulse in HMM for (a) unchirped ($\beta = 0$) and (b) chirped ($\beta = 3$) cases.

The calculated dependence of the delay of the pulse maximum in the HMM, $\tau(\lambda, \theta)$, for unchirped laser pulse ($\beta = 0$) are shown in Fig. 3(a). Here the retardation of pulse in the vacuum slab with thickness L_{HMM} is already subtracted. We found the peculiar change of the delay in HMM with pronounced negative and positive values indicating the fast-slow light effect in agreement with the experimental results [Fig. 2(b)]. The pulse advance achieves the values up to 50 fs and the retardation of 37 fs near the “A” specific spectral point in Fig. 3(a). We note that the measured delays are smaller than the simulated ones that is caused by smearing of transmission dips for the experimental HMM due to the long-range deviation of the periodicity intrinsic to the AAO and the variation of silver nanorod length L_{HMM} .

We address that for unchirped radiation, the change of the angle of incidence results in the transition between the two dynamical effects, paving a route towards HMM-based delay line for ultrafast optics. Another picture of the delay tuning appears for chirped laser pulses. Interestingly, the positive pulse chirp ($\beta = 3$) leads to a counterclockwise rotation of the fast-slow light transition region in the $\lambda - \theta$ map, shown by an arrow, and boosts the strength of the fast-slow light effect [Fig. 3(b)]. The latter originates from the increase in pulse duration by $\sqrt{1 + \beta^2}$ times compared to the case $\beta = 0$.

The calculated $\lambda - \theta$ dependence of the HMM transmission is shown in Fig. 4(a), disclosing a set of local minima near $\lambda_{\text{ENZ}} = 760 \text{ nm}$, in which the transmission drops to zero. We found that enhancement of both the pulse advance and its delay shown in Fig. 3 are attributed to these minima,

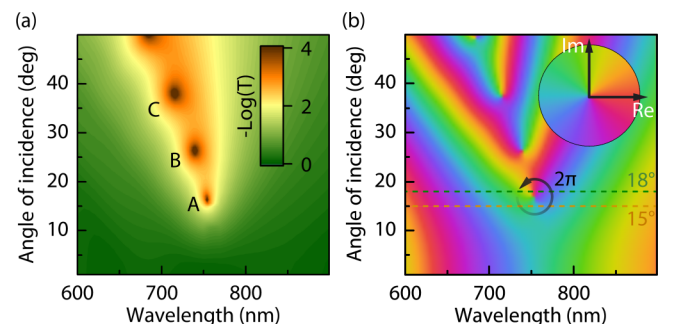


FIG. 4. (a) Calculated $\lambda - \theta$ dependence of light transmission (T) of HMM. (b) Calculated phase φ of the complex field transmission coefficient (t).

underpinning the experimental observations [Fig. 2]. We stress that usage of the effective medium model with neglected nonlocality to emulate optical properties of the nanocomposite does not provide both an observed set of transmission dips near the ENZ and the resonant fast-slow light effect that demonstrates the paramount importance of the nonlocality in observed phenomena (Sec. I in Supplemental Material [49]).

B. Dispersion of eigenmodes and optical nonlocality of HMM

In order to give a physical picture of the revealed fast-slow light effects and their relation to HMM nonlocality we first provide insight into the spatial dispersion of light in the silver nanorod-based HMM. To do so, using the finite element method (FEM) through the application of COMSOL software we calculated the eigenmodes of light in a hexagonal lattice of infinitely long silver nanorods in AAO with the parameters listed above [Fig. 1(b)]. In the modeling special attention was paid to the optical properties of the constituent materials. For AAO we assumed the refractive index of $n_{AAO} = 1.55$ in accordance with Ref. [59], which is smaller as compared to that of crystalline alumina. Additionally, this value was checked by comparison of the measured $\Delta t = 84$ fs difference of laser pulse delays in the AAO template with the thickness L_{AAO} and in the air slab of the same thickness, and calculated difference given by $\Delta t = (n_{\text{eff}} - 1)L_{AAO}/c = 83$ fs. In the case of AAO-air composite with the porosity of f the effective refractive index n_{eff} is obtained via the Maxwell-Garnett effective medium approximation [60]. For silver nanorods we applied the following model for their permittivity [48]:

$$\varepsilon(\omega) = \varepsilon_{\text{bulk}} + \frac{i\omega_p^2\tau(R_b - R)}{\omega(\omega\tau + i)(\omega\tau R + iR_b)}, \quad (4)$$

in which the bulk permittivity of metal $\varepsilon_{\text{bulk}}$ suffers correction stemming from the diminishing of the electron mean free path R in deposited metals compared with that for bulk metal R_b . We used $R_b = 40$ nm, the plasma frequency $\omega_p = 8.9$ eV/ \hbar , and electron relaxation time $\tau = 3.1 \times 10^{-14}$ s specific for bulk silver [61,62]. The correction term increases predominantly the optical absorption and slightly affects the real part of metal permittivity. We assumed the mean free path of the conduction electrons equal to $R = 4$ nm, which is a typical value for electrodeposited metal nanorods [48,63] and provides good matching of the experimental and calculated values of the HMM light attenuation.

Carried out FEM calculations demonstrate that the structure sustains the propagation of three Bloch eigenmodes in the considered spectral range. It is in contrast to the results of the common approach of the local anisotropic effective medium, e.g., the Maxwell-Garnett approximation resulting in two optical waves, ordinary and extraordinary [48]. The total forward propagating optical electric field in the HMM is a superposition of three eigenmodes,

$$\mathbf{E}(\mathbf{r}) = \sum_{j=1,2,3} a^{(j)} \mathcal{E}^{(j)}(x, y) \exp(ik_z^{(j)}z) \exp(ik_x x + ik_y y), \quad (5)$$

where k_x, k_y are the Bloch wave numbers; $\mathcal{E}^{(j)}(x, y)$ is the spatial distribution of vectorial electric field of the eigenmode j and $a^{(j)}, k_z^{(j)}$ are its amplitude and the complex propagation

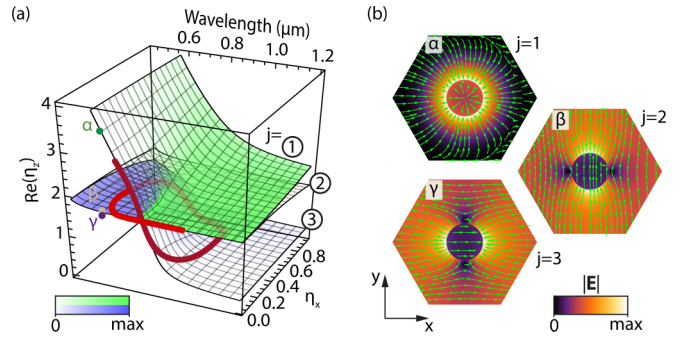


FIG. 5. (a) Dispersion of three eigenmodes of light in the HMM. Circled labels indicate serial numbers of the eigenmodes (j). The color saturation indicates the amplitudes of the eigenmodes excited by incident p -polarized plane wave. Red curve shows the path of continuous change of the eigenmode field distributions. (b) Spatial distribution of the amplitudes of the electric field of three eigenmodes 1, 2, 3 in points α , β , γ , respectively, in the HMM primitive unit cell. Green arrows are streamlines of the electric field vector.

constant; and the z axis is oriented along silver nanorods. For convenience we introduce dimensionless wave numbers $\eta_x = k_x/k_0$ and $\eta_z^{(j)} = k_z^{(j)}/k_0$, where $k_0 = \omega/c$ is the vacuum wave number. In simulations we assumed $k_y = 0$.

The spectral-angular dependencies of $Re(\eta_z^{(j)})$ obtained via FEM are shown in Fig. 5(a), where the dispersion sheets are numbered by the index j in the descending order of $Re(\eta_z^{(j)})$. Far away from the ENZ wavelength two eigenmodes are the main waves, which correspond to the ordinary and extraordinary waves in the case of a homogenized uniaxial composite. In the near-infrared spectral region they are $j = 1, 2$, the former of which ($j = 1$) possesses hyperbolic dispersion, while for the short wavelengths two main eigenmodes, $j = 2, 3$, demonstrate elliptic dispersion with the associated decrease of $Re(\eta_z^{(j)})$ with the growth of η_x . Figure 5(b) demonstrates the spatial distribution of the electric field of eigenmodes, $\mathcal{E}^{(j)}(x, y)$, in the spectral-angular points α , β , and γ attributed to the sheets $j = 1, 2, 3$, respectively [Fig. 5(a)]. As seen, the main eigenmodes $j = 2, 3$ demonstrate the specific dipolelike response of the metal cylinder to the transverse electric field oriented along the y and x axes. As the result, the HMM optical properties beyond the ENZ wavelength are described well by local Maxwell-Garnett effective medium approximation [11,33].

Besides the two main eigenmodes, the nanocomposite supports the propagation of the additional eigenmode ($j = 1$ for $\lambda < \lambda_{\text{ENZ}}$ and $j = 3$ for $\lambda > \lambda_{\text{ENZ}}$), indicating the spatial dispersion of the metamaterial [15] and associated with the cylindrical plasmon propagating in Ag nanorods. The specific radial distribution of the electric field of this longitudinal eigenmode is shown in Fig. 5(b) for the point α of Fig. 5(a). It is important to note that at normal propagation $\eta_x = 0$ the dispersions of eigenmodes $j = 1, 3$ are crossing at the ENZ spectral point; the inclined propagation $\eta_x \neq 0$ results in (i) avoiding crossing of their dispersion sheets, i.e., relative repulsion of spectra of $Re(\eta_z^{(1)})$, $Re(\eta_z^{(3)})$ [see Fig. 5(a)] and (ii) related hybridization of main and additional modes ($j = 1, 3$). As seen, the main mode $j = 2$ associated with ordinary wave

in a uniaxial crystal does not participate in the hybridization [Fig. 5(a)]. The mode-mixing is illustrated in Fig. 5(a) by a red curve indicating the continuous change of eigenmode field distribution for two hybridized dispersion surfaces ($j = 1, 3$) “glued” near $\eta_x = 0$ at λ_{ENZ} .

The described specifics of the dispersion surfaces indicate the strong effect of nonlocality of the optical response and related HMM spatial dispersion. Indeed, the appearance of the additional eigenmode and avoiding crossing the dispersions of eigenmodes shown above is reproduced well by the dispersion equation

$$\frac{\eta_x^2}{\varepsilon_e + \alpha\eta_z^2} + \frac{\eta_z^2}{\varepsilon_o} = 1 \quad (6)$$

when considering the Maxwell-Garnett medium of the composites with the effective ordinary (ε_o) and extraordinary (ε_e) permittivities and the spatial dispersion correction of the latter by the parameter $|\alpha| \approx 0.13$. The dispersion sheets obtained via solution of Eq. (6) are shown in Sec. II of the Supplemental Material [49].

C. Nonlocality effect in light transmission through HMM

In natural nonlocal media the spatial dispersion could have a significant effect on the light transmission due to the interference of the main and additional eigenmodes [34]. The light propagation through the HMM with the spatial dispersion was calculated by solving the appropriate boundary problem. Namely, for both HMM interfaces we (i) required the continuity of the tangential components of the electric $\langle E_{x,y} \rangle$ and magnetic $\langle H_{x,y} \rangle$ fields averaged over the primitive unit cell, and (ii) imposed additional boundary conditions necessary to treat a nonlocal media. The latter were taken in the form of the continuity of the Fourier components $\langle D_z \exp(-i\mathbf{G}\mathbf{r}) \rangle$ and $\langle E_x \exp(-i\mathbf{G}\mathbf{r}) \rangle$, where $\mathbf{G} = 4\pi/\sqrt{3}(1, 0)^T$ is the reciprocal lattice vector [64]. This approach was applied to obtain the complex field transmission coefficient $t(\omega, \theta)$ harnessed in Eq. (3) for the calculation of the laser pulse propagation in a HMM slab.

In Fig. 5(a) we demonstrate by color saturation the obtained amplitudes $a^{(j)}$ [see Eq. (5)] of the eigenmodes excited in the HMM under oblique incidence of the p -polarized plane wave. As seen, beyond the ENZ wavelength or at normal incidence, solely the main eigenmode associated with the extraordinary wave is excited (see bright colors at $\eta_x = 0$), while the excitation of the additional one is prohibited by the difference of the symmetries of the field distributions of the incident plane wave and the additional eigenmode [Fig. 5(b)]. Being TE polarized, the eigenmode $j = 2$ is not excited by the incident p -polarized wave.

In turn, due to eigenmode hybridization the ENZ afforded simultaneous excitation of the main and additional eigenmodes ($j = 1, 3$) in the HMM under oblique incidence of the p -polarized plane wave [Fig. 5(a)]. We assert that near the ENZ wavelength their amplitudes become comparable, resulting in vivid interference features of the light transmission through the HMM shown in Fig. 4(a). As seen, besides the decrease of the HMM transmittance specific to the ENZ regime and mediated by hybridization of the main and additional waves, a set of pronounced minima occurs with sharp

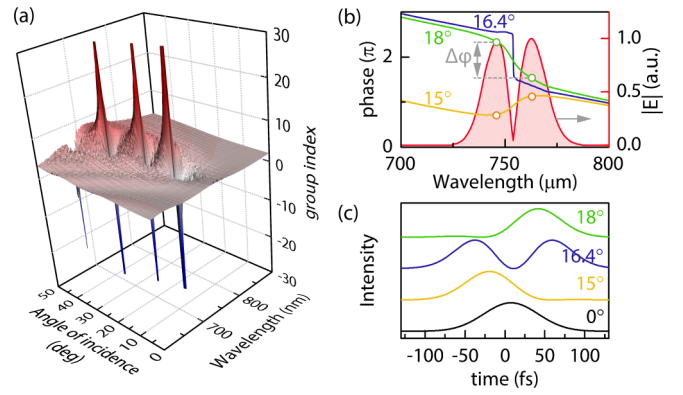


FIG. 6. (a) Calculated spectral-angular dependence of group index of light in HMM. (b) The spectra of amplitude of electric field of transmitted laser pulse for $\theta = 16.4^\circ$ (red) and the phases of complex transmission coefficient of HMM for incident angles $\theta = 15^\circ, 16.4^\circ$, and 18° . (c) Temporal dependencies of intensity of transmitted laser pulses for four angles of incidence.

drops of the transmittance. They correspond to the destructive interference of the main and additional waves with the numbers $j = 1, 3$. The calculated $\lambda - \theta$ positions of the minima correspond well to the experimental spectra [Fig. 2(a)], while nonzero transmittance in the experiment is due to the variation of length of the nanorods L_{HMM} and interrod spacing a . We stress that the intermode interference within the HMM differs from that in thin film where the interference fringes appear with commonly nonunit visibility. In contrast, HMM afforded exactly zero transmittance in the spectral points A, B, and C shown in Fig. 4(a). It appears inevitable due to growing and diminishing of the spectral dependencies of the eigenmode amplitudes at the output HMM interfaces $|a^{(1)} \exp(-\text{Im}(k_z^{(1)})L_{\text{HMM}})|$ and $|a^{(3)} \exp(-\text{Im}(k_z^{(3)})L_{\text{HMM}})|$.

D. Transmission phase singularities in fast-slow light effect

Zero transmittance results in the phase singularity of $t(\omega, \theta)$, where $\varphi = \arg[t(\omega, \theta)]$ is undefined. Recently phase singularities conquered the realm of photonics for the generation of optical vortex beams [65], superoscillations [66], and perfect absorption in plasmon antenna array [67], to name but a few. However, to the best of our knowledge, they have not been discussed in optics of HMMs to date. We illustrate singularities in HMM transmittance in Fig. 4(b) where a $\lambda - \theta$ map of the phase φ is shown. Near the zero values of $t(\omega, \theta)$ the phase changes continuously, accumulating 2π in the clockwise direction. The related topological charge of the phase singularity $C = 1/(2\pi) \oint \nabla\varphi \cdot d\mathbf{l}$ computed for the enclosing loop takes the value of unity and is the same for each singularity. We assert it is the 2π phase swing in the singularity points that furnishes the fast-slow light effect. We demonstrate this in Fig. 6(a), which shows the $\lambda - \theta$ map of the group index (n_g) obtained as $n_g = (c/L_{\text{HMM}}) \partial\varphi/\partial\omega$. As seen, it demonstrates both large positive and negative values, which appear close to zero transmission points. The first case corresponds to the slow light effect and the values $n_g < 1$ indicate superluminality. The revealed group index features are in agreement with the experimental and numerical

manifestations of these phenomena in the propagation of femtosecond laser pulses through HMMs [Figs. 2(b) and 3].

We assert that the peculiar resonant change of the group index in the $\lambda - \theta$ map and related fast and slow light effects originate from the rapid change of the phase φ near the singularity points. It is demonstrated in Fig. 6(b) by orange and green curves, which are the spectral dependencies of φ of transmitted wave for two angles of incidence $\theta = 15^\circ$ and 18° , which are smaller and larger than the angular position of the singularity point [see dashed lines in Fig. 4(b)]. The first curve experiences anomalous dispersion near the ENZ wavelength, resulting in superluminal light propagation, while the second curve demonstrates increased normal dispersion, yielding the slow light effect. When approaching the critical angle of singularity ($\theta = 16.4^\circ$), the spectral variation of φ undergoes an extremely high gradient [see blue curve in Fig. 6(b)], giving rise to singularities in the group index that can be seen in Fig. 6(a). We stress that the phase jump and group index variation near the singularity point can be further increased by stacking several identical HMM films separated by air gaps.

Recently, phase singularities were harnessed for pulse manipulation in other physical systems. In radio frequency range it results in superluminal and slow light effects (i) in birefringent photonic crystals [68] and (ii) in the yttrium iron garnet-microstrip cavity system due to multiple-path interference of guided microwave, magnon, and resonator state [69]. In optics anomalously large time delay of the laser pulse in a waveguide coupled to a ring resonator was demonstrated under near-zero transmission [70]. The phase jump close to the singularity points inspired the superoscillation concept for superseding the diffraction limit in microscopy [66,71].

E. Relaxation of group index singularities

It should be noted that the finite spectral width of the incident pulse prevents infinite values of the pulse delay/advance $\tau = (n_g - 1)L_{\text{HMM}}/c$ in the HMM when n_g goes to infinity [Fig. 6(a)]. It takes place inevitably in the close vicinity of the singularity points when the spectral width of the phase jump region is comparable to or less than the spectral width of the laser pulse. As a result, the spectrum of the transmitted pulse has a two-bell shape as shown by the red shaded area in Fig. 6(b) that is caused by zero transmission of HMM under the destructive interference of the main and additional waves as described above. We address special attention to this tricky case. Near the zero-transmission point the complex transmission coefficient could be approximated by the linear function $t(\omega, \theta_0) = \xi(\omega - \omega_0)$, where θ_0 and ω_0 are the angle of incidence and frequency of the destructive interference point. In the time domain this Fourier factor [see Eq. (3)] is equivalent to the temporal differentiation (d/dt) of the pulse envelope leading to two bell-shaped temporal dependence of the transmitted pulse intensity, as illustrated by the blue curve in Fig. 6(c) for $\theta_0 = 16.4^\circ$, i.e., point A in Fig. 4(a). In this case the first peak of the transmitted pulse is advanced, while the second one is delayed that mimics both fast and slow light effects. As seen, the finite spectral width of the laser pulse

cures infinite advance/delay related to the n_g divergence. The value τ , however, could tend to rise when the duration of the incident pulse is increasing. For other angles θ near the zero-transmission points the pulse shape can be considered as the result of the intrapulse interference of two distant spectral bands [see red area in Fig. 6(b)]. Indeed, after propagation through the HMM they acquire the phase difference $\Delta\varphi$, which depends on θ [Fig. 6(b)], and the pulse spectrum could be described qualitatively as

$$E_{\text{inc}}(\omega)t(\omega, \theta) \approx A \exp(i\Delta\varphi) \exp[-(\omega - \omega_1)^2/\delta^2] + \exp[-(\omega - \omega_2)^2/\delta^2], \quad (7)$$

where ω_1, ω_2 are the frequencies of the maxima of the transmitted pulse spectrum [red area in Fig. 6(b)]. As a result, the interference terms appear in the temporal dependence of the pulse intensity [see Eq. (3)],

$$I(t) \approx \exp(-\delta^2 t^2/2) [1 + A^2 + 2A \cos(\Delta\varphi + (\omega_2 - \omega_1)t)]. \quad (8)$$

The temporal position of the maximum of this function depends on $\Delta\varphi$. When changing the sign of $\Delta\varphi$ under variation of θ , a superluminal pulse peak advance or delay appears for the femtosecond laser radiation as illustrated by orange and green curves in Fig. 6(c) for $\theta = 15^\circ$ and 18° related to negative and positive $\Delta\varphi$, respectively.

IV. CONCLUSIONS

Summing up, we revealed experimentally and theoretically the superluminal and slow propagation of femtosecond laser pulses in the HMM based on an array of silver nanorods in an alumina template. It is found that these dynamical phenomena occur in the ENZ regime of the HMM and originate from strong optical nonlocality of the considered composite in this spectral range. The latter gives rise to zero transmission of the HMM driven by the destructive interference of the main and additional eigenmodes of light in the metamaterial, resulting in phase singularity points, which are the heart of the observed phenomena, providing anomalous or strong normal dispersion of light. It is demonstrated that fast-slow light effect in HMM can be tuned by variation of the angle of incidence of light pulses or of the central wavelength of a chirped pulse. The revealed dynamical phenomena provide a venue harnessing the nonlocality for the manipulation of ultrashort laser pulses and can be of primary importance in applications of all-optical switching of femtosecond pulses. We believe that the proposed nonlocality-based approach could be extended for other photonic systems for the control of ultrashort laser pulses. Moreover, we assert that phase singularities of the HMM transmittance revealed here open a simple method for the generation of astonishing spatiotemporal optical vortices [72–74] using thin HMM film exclusively, as will be described in our forthcoming paper.

ACKNOWLEDGMENT

This work is supported by the Russian Science Foundation under Grant No. 19-72-00118.

- [1] Z. Jacob, J.-Y. Kim, G. V. Naik, A. Boltasseva, E. E. Narimanov, and V. M. Shalaev, *Appl. Phys. B* **100**, 215 (2010).
- [2] I. A. Kolmychek, V. B. Novikov, I. V. Malysheva, A. P. Leontiev, K. S. Napolskii, and T. V. Murzina, *Opt. Lett.* **45**, 1866 (2020).
- [3] D. Lu and Z. Liu, *Nat. Commun.* **3**, 1 (2012).
- [4] T. Repän, A. V. Lavrinenko, and S. V. Zhukovsky, *Opt. Express* **23**, 25350 (2015).
- [5] X. Chen, C. Zhang, F. Yang, G. Liang, Q. Li, and L. J. Guo, *ACS Nano* **11**, 9863 (2017).
- [6] J. Zhou, A. F. Kaplan, L. Chen, and L. J. Guo, *ACS Photon.* **1**, 618 (2014).
- [7] A. Alù, M. G. Silveirinha, A. Salandrino, and N. Engheta, *Phys. Rev. B* **75**, 155410 (2007).
- [8] I. A. Kolmychek, A. R. Pomozov, V. B. Novikov, A. P. Leontiev, K. S. Napolskii, and T. V. Murzina, *Opt. Express* **27**, 32069 (2019).
- [9] A. Poddubny, I. Iorsh, P. Belov, and Y. Kivshar, *Nat. Photon.* **7**, 948 (2013).
- [10] M. G. Silveirinha, *Phys. Rev. E* **73**, 046612 (2006).
- [11] T. Geng, S. Zhuang, J. Gao, and X. Yang, *Phys. Rev. B* **91**, 245128 (2015).
- [12] R.-L. Chern, *Opt. Express* **21**, 16514 (2013).
- [13] J. Elser, R. Wangberg, V. A. Podolskiy, and E. E. Narimanov, *Appl. Phys. Lett.* **89**, 261102 (2006).
- [14] B. Wells, Z. A. Kudyshev, N. Litchinitser, and V. A. Podolskiy, *ACS Photon.* **4**, 2470 (2017).
- [15] V. M. Agranovich and V. Ginzburg, *Crystal Optics with Spatial Dispersion, and Excitons* (Springer, New York, 2013), Vol. 42.
- [16] B. Gompf, J. Braun, T. Weiss, H. Giessen, M. Dressel, and U. Hübner, *Phys. Rev. Lett.* **106**, 185501 (2011).
- [17] J. Pastrnak and K. Vědem, *Phys. Rev. B* **3**, 2567 (1971).
- [18] A. A. Orlov, P. M. Voroshilov, P. A. Belov, and Y. S. Kivshar, *Phys. Rev. B* **84**, 045424 (2011).
- [19] C.-W. Chen, T. Bian, H.-P. Chiang, and P. T. Leung, *J. Opt.* **18**, 025104 (2016).
- [20] V. Popov, A. V. Lavrinenko, and A. Novitsky, *Phys. Rev. B* **97**, 125428 (2018).
- [21] L. Sun, J. Gao, and X. Yang, *Opt. Express* **21**, 21542 (2013).
- [22] V. Popov, A. V. Lavrinenko, and A. Novitsky, *Phys. Rev. B* **94**, 085428 (2016).
- [23] C. R. Simovski, P. A. Belov, A. V. Atrashchenko, and Y. S. Kivshar, *Adv. Mater.* **24**, 4229 (2012).
- [24] W. Yan, N. A. Mortensen, and M. Wubs, *Opt. Express* **21**, 15026 (2013).
- [25] H. Hu, X. Lin, J. Zhang, D. Liu, P. Genevet, B. Zhang, and Y. Luo, *Laser Photon. Rev.* **14**, 2000149 (2020).
- [26] F. Liu, L. Xiao, Y. Ye, M. Wang, K. Cui, X. Feng, W. Zhang, and Y. Huang, *Nat. Photon.* **11**, 289 (2017).
- [27] K. J. Lee, Y. U. Lee, F. Fages, J.-C. Ribierre, J. W. Wu, and A. D'Aléo, *Nano Lett.* **18**, 1476 (2018).
- [28] K. J. Lee, Y. Xiao, J. H. Woo, E. Kim, D. Kreher, A.-J. Attias, F. Mathevet, J.-C. Ribierre, J. W. Wu, and P. André, *Nat. Mater.* **16**, 722 (2017).
- [29] D. Correas-Serrano, J. S. Gomez-Diaz, M. Tymchenko, and A. Alù, *Opt. Express* **23**, 29434 (2015).
- [30] S. S. Kruk, D. A. Powell, A. Minovich, D. N. Neshev, and Y. S. Kivshar, *Opt. Express* **20**, 15100 (2012).
- [31] B. Fan, D. Filonov, P. Ginzburg, and V. A. Podolskiy, *Opt. Express* **26**, 17541 (2018).
- [32] V. M. Agranovich and V. L. Ginzburg, *Sov. Phys.-Usp.* **5**, 323 (1962).
- [33] R. J. Pollard, A. Murphy, W. R. Hendren, P. R. Evans, R. Atkinson, G. A. Wurtz, A. V. Zayats, and V. A. Podolskiy, *Phys. Rev. Lett.* **102**, 127405 (2009).
- [34] M. Brodin and S. Pekar, *J. Exp. Theor. Phys* **11**, 1373 (1960).
- [35] F. Hu, L. Li, Y. Liu, Y. Meng, M. Gong, and Y. Yang, *Commun. Phys.* **4**, 84 (2021).
- [36] P. Ginzburg, F. J. Rodríguez Fortuño, G. A. Wurtz, W. Dickson, A. Murphy, F. Morgan, R. J. Pollard, I. Iorsh, A. Atrashchenko, P. A. Belov, Y. S. Kivshar, A. Nevet, G. Ankonina, M. Orenstein, and A. V. Zayats, *Opt. Express* **21**, 14907 (2013).
- [37] A. D. Neira, N. Olivier, M. E. Nasir, W. Dickson, G. A. Wurtz, and A. V. Zayats, *Nat. Commun.* **6**, 7757 (2015).
- [38] P. Kelly and L. Kuznetsova, *OSA Continuum* **3**, 3225 (2020).
- [39] L. H. Nicholls, F. J. Rodríguez-Fortuño, M. E. Nasir, R. M. Córdova-Castro, N. Olivier, G. A. Wurtz, and A. V. Zayats, *Nat. Photon.* **11**, 628 (2017).
- [40] B. Li, Y. He, and S. He, *Appl. Phys. Express* **8**, 082601 (2015).
- [41] S. Liang, C. Jiang, Z. Yang, D. Li, W. Zhang, T. Mei, and D. Zhang, *J. Opt.* **20**, 065001 (2018).
- [42] A. D. Neira, G. A. Wurtz, and A. V. Zayats, *Sci. Rep.* **5**, 1 (2015).
- [43] E. Yoxall, M. Schnell, A. Y. Nikitin, O. Txoperena, A. Woessner, M. B. Lundeberg, F. Casanova, L. E. Hueso, F. H. Koppens, and R. Hillenbrand, *Nat. Photon.* **9**, 674 (2015).
- [44] V. B. Novikov, A. P. Leontiev, K. S. Napolskii, and T. V. Murzina, *Opt. Lett.* **46**, 2276 (2021).
- [45] T. Stefaniuk, L. H. Nicholls, R. M. Córdova-Castro, M. E. Nasir, and A. V. Zayats, *Adv. Mater.* 2107023 (2022).
- [46] I. A. Kolmychek, I. V. Malysheva, V. B. Novikov, A. P. Leontiev, K. S. Napolskii, and T. V. Murzina, *Phys. Rev. B* **102**, 241405(R) (2020).
- [47] I. V. Roslyakov, E. O. Gordeeva, and K. S. Napolskii, *Electrochim. Acta* **241**, 362 (2017).
- [48] R. Atkinson, W. R. Hendren, G. A. Wurtz, W. Dickson, A. V. Zayats, P. Evans, and R. J. Pollard, *Phys. Rev. B* **73**, 235402 (2006).
- [49] See Supplemental Material at <http://link.aps.org/supplemental/10.1103/PhysRevB.106.165415> for effective permittivity of the HMM, spectra of the light transmission and pulse delay for local effective medium of the nanocomposite, dispersion of the eigenmodes in nonlocal effective medium.
- [50] M. D. Stenner, D. J. Gauthier, and M. A. Neifeld, *Nature (London)* **425**, 695 (2003).
- [51] F. R. Faxvog, C. N. Y. Chow, T. Bieber, and J. A. Carruthers, *Appl. Phys. Lett.* **17**, 192 (1970).
- [52] S. Chu and S. Wong, *Phys. Rev. Lett.* **48**, 738 (1982).
- [53] A. M. Akulshin, A. Cimmino, and G. I. Opat, *Quantum Electron.* **32**, 567 (2002).
- [54] A. M. Akulshin, S. Barreiro, and A. Lezama, *Phys. Rev. Lett.* **83**, 4277 (1999).
- [55] G. M. Gehring, A. Schweinsberg, C. Barsi, N. Kostinski, and R. W. Boyd, *Science* **312**, 895 (2006).
- [56] L. Thévenaz, *Nat. Photon.* **2**, 474 (2008).
- [57] L. Wang, A. Kuzmich, and A. Dogariu, *Nature (London)* **406**, 277 (2000).
- [58] S. A. Akhmanov, V. A. Vysloukh, A. S. Chirkin, and Y. Atanov, *Optics of Femtosecond Laser Pulses* (Springer, New York, 1992).

- [59] A. Hierro-Rodriguez, P. Rocha-Rodrigues, F. Valdés-Bango, J. M. Alameda, P. A. S. Jorge, J. L. Santos, J. P. Araujo, J. M. Teixeira, and A. Guerreiro, *J. Phys. D* **48**, 455105 (2015).
- [60] V. A. Markel, *J. Opt. Soc. Am. A* **33**, 1244 (2016).
- [61] P. B. Johnson and R. W. Christy, *Phys. Rev. B* **6**, 4370 (1972).
- [62] H. Kanter, *Phys. Rev. B* **1**, 522 (1970).
- [63] S. Peruch, A. Neira, G. A. Wurtz, B. Wells, V. A. Podolskiy, and A. V. Zayats, *Adv. Opt. Mater.* **5**, 1700299 (2017).
- [64] B. M. Wells, A. V. Zayats, and V. A. Podolskiy, *Phys. Rev. B* **89**, 035111 (2014).
- [65] Y. Shen, X. Wang, Z. Xie, C. Min, X. Fu, Q. Liu, M. Gong, and X. Yuan, *Light Sci. Appl.* **8**, 90 (2019).
- [66] G. Yuan, E. T. Rogers, and N. I. Zheludev, *Light Sci. Appl.* **8**, 2 (2019).
- [67] A. Berkhout and A. F. Koenderink, *ACS Photon.* **6**, 2917 (2019).
- [68] D. R. Solli, C. F. McCormick, R. Y. Chiao, S. Popescu, and J. M. Hickmann, *Phys. Rev. Lett.* **92**, 043601 (2004).
- [69] Z. Lu, Q. Zhang, Y. Sun, Y. Chen, Y. Tian, S. Yan, and L. Bai, *J. Magn. Magn. Mater.* **546**, 168868 (2022).
- [70] M. Asano, K. Y. Bliokh, Y. P. Bliokh, A. G. Kofman, R. Ikuta, T. Yamamoto, Y. Kivshar, L. Yang, N. Imoto, Ş. Özdemir, and F. Nori, *Nat. Commun.* **7**, 13488 (2016).
- [71] M. Berry, N. Zheludev, Y. Aharonov, F. Colombo, I. Sabadini, D. C. Struppa, J. Tollaksen, E. T. F. Rogers, F. Qin, M. Hong, X. Luo, R. Remez, A. Arie, J. B. Götte, M. R. Dennis, A. M. H. Wong, G. V. Eleftheriades, Y. Eliezer, A. Bahabad, G. Chen, Z. Wen, G. Liang, C. Hao, C.-W. Qiu, A. Kempf, E. Katzav, and M. Schwartz, *J. Opt.* **21**, 053002 (2019).
- [72] N. Jhajj, I. Larkin, E. W. Rosenthal, S. Zahedpour, J. K. Wahlstrand, and H. M. Milchberg, *Phys. Rev. X* **6**, 031037 (2016).
- [73] A. Chong, C. Wan, J. Chen, and Q. Zhan, *Nat. Photon.* **14**, 350 (2020).
- [74] J. Huang, J. Zhang, T. Zhu, and Z. Ruan, *Laser Photon. Rev.* **16**, 2100357 (2022).